Sensors and Materials, Vol. 37, No. 2 (2025) 487–495
MYU Tokyo

S & M 3924

X-ray-induced Luminescence Properties of Eu-doped Alkaline Earth Borate Glasses

Hiroyuki Fukushima,[1*] Ren Tsubouchi,[2] Toru Matsuura,[1]
Tomoaki Yoneda,[1] and Takayuki Yanagida[2]

[1]Department of Electrical and Electronic Engineering, National Institute of Technology, Fukui College, Geshi, Sabae, Fukui 916-8507, Japan
[2]Division of Materials Science, Nara Institute of Science and Technology, 8916-5 Takayama-cho, Ikoma, Nara 630-0192, Japan

(Received October 31, 2024; accepted December 18, 2024)

Keywords: photoluminescence, scintillation, Eu-doped glass

The photoluminescence and scintillation properties of Eu-doped (0.1, 1, 5, and 10 mol%) $CaO–Al_2O_3–B_2O_3$ glasses were investigated. The photoluminescence spectra showed sharp emission peaks at ~600 nm owing to the 4f–4f transitions of Eu^{3+}. The X-ray-induced scintillation spectra were also similar to those observed in photoluminescence. The photoluminescence quantum yield reached 96% in the 10% Eu-doped sample. The photoluminescence and X-ray-induced scintillation decay curves were clearly observed, and the decay time constants were of 1 ms order.

1. Introduction

Ionizing radiations such as α-, β-, γ-, and X-rays have high energy. Above all, X-rays and γ-rays have high penetration power, and these are utilized to inspect objects nondestructively, such as the human body and luggage. Scintillators to detect ionizing radiation are used in various applications. Scintillators convert the energy of ionizing radiation to low-energy photons of light emission. Scintillation consists of three essential steps leading to photon emission. First, the primary electron is ionized when scintillators absorb the energy of ionizing radiation. The energized primary electron is scattered with a host lattice, and the secondary electrons are generated. Second, these electrons and holes are transferred to luminescence centers. Finally, the electrons and holes are recombined at luminescence centers. As mentioned earlier, the applications of scintillators include nondestructive inspection processes such as X-ray computed tomography,[(1)] positron emission tomography (PET),[(2)] luggage inspection,[(3)] environmental monitoring,[(4)] and well logging.[(5)] The desired properties of scintillators are high light yield, fast decay time, low afterglow, and chemical and physical stability.[(6)] There are many commercially available scintillators, and users select suitable scintillators in accordance with their applications. For instance, $Bi_4Ge_3O_{12}$ single crystals have been used as scintillators for PET.[(7)] In recent years,

*Corresponding author: e-mail: fukushima@fukui-nct.ac.jp
https://doi.org/10.18494/SAM5438

ISSN 0914-4935

$Bi_4Ge_3O_{12}$ single crystals have been replaced with Ce-doped Lu_2SiO_5 single crystals for PET scintillators.[8] To develop novel scintillators, researchers have investigated the scintillation properties of single crystals,[9–21] ceramics,[22–27] and glasses.[28–34]

The lithium glass scintillator (GS20) has been developed for neutron detection, and the light yield under ^{137}Cs γ-ray irradiation is 4000 photons/MeV.[35] GS20 is one of the few commercially available glass scintillators. Many glasses have been investigated to develop a novel glass scintillator for the detection of neutron, α-, X-, and γ-rays.[36] However, glasses exhibit relatively low scintillation intensity and light yield, and the reason is attributed to the low efficiency of carrier transfer from a host to a luminescence center owing to the structure of glass.[36] In addition, glass is composed of light elements such as SiO_2, B_2O_3, P_2O_5, and GeO_2. The detection efficiencies of X- and γ-rays roughly depend on the density and effective atomic number of materials.[2] The weak points of glass scintillators can be overcome by including a high concentration of luminescence centers, especially rare-earth ions. The density and effective atomic number of glasses increase with the concentration of rare-earth ions. For instance, glasses doped with Ce^{3+} at more than 10 mol% show a relatively high light yield of up to 3200 photons/MeV under ^{137}Cs γ-ray irradiation.[37] Moreover, the scintillation properties of other high-Ce^{3+}-concentration glasses have been investigated.[38–40] More importantly, these glasses with high Ce^{3+} concentrations exhibit a high quantum yield (QY). Usually, concentration quenching is observed in materials with a high concentration of luminescence centers. In contrast, some materials show high QY even in the high-dopant-concentration region. The scintillation process includes luminescence at the luminescence center; thus, the scintillation intensity depends on the QY at the luminescence center. Therefore, we are interested in high-QY glasses with high rare-earth-ion doping concentration as novel glass scintillators, and CaO–Al_2O_3–B_2O_3 glass is one of the candidates.

The scintillation and dosimetric properties of rare-earth-doped CaO–Al_2O_3–B_2O_3 glasses have been investigated.[41–43] Among them, Ce-doped glass exhibited a high QY of ~60%, and Tb-doped glass exhibited a similar luminescence intensity from 1 to 5 mol%; thus, these glasses may possibly have a high QY with a high concentration of luminescence centers. As a luminescence center, Eu is selected in this study. Eu-doped materials show luminescence at ~600 nm owing to the 4f–4f transitions of Eu^{3+}. The typical wavelength sensitivity of the bialkali-type photomultiplier tube is unsuitable for red emissions at ~600 nm. In contrast, the wavelength sensitivity of the Si photodiode is suitable for red emissions; thus, the scintillation properties of materials with red emissions have been investigated.[44–46] In this study, the luminescence properties of Eu-doped 30CaO-20Al_2O_3–50B_2O_3 glasses under UV and X-ray irradiations were investigated.

2. Materials and Methods

Eu-doped 30CaO-20Al_2O_3–50B_2O_3 glasses were prepared by the conventional melt-quenching method. The powders used were $CaCO_3$ (99.99%, High Purity Chemicals), Al_2O_3 (99.9%, High Purity Chemicals), H_3BO_3 (99.99%, High Purity Chemicals), and Eu_2O_3 (99.9%, High Purity Chemicals). The nominal concentrations of Eu were 0.1, 1, 5, and 10 mol%. These

powders were mixed using a mortar and pestle for 15 min. The mixture was put into an alumina crucible, and then placed into an electric furnace. The temperature of the electric furnace was 1100 °C, and the melting time was 1 h for every sample. The melted mixture was poured onto a stainless-steel plate heated to 400 °C, and then quickly pressed using another heated stainless-steel plate.

The X-ray diffraction (XRD) patterns were measured using a powder of crushed samples (Ultima IV, Rigaku). The photoluminescence (PL) spectra were measured using a spectrometer (QE2100, Otsuka electronics). The range of excitation wavelengths was 250–400 nm. The PL QY was also measured using a spectrometer (Hamamatsu Photonics, C11347). The PL decay curves were also measured using another spectrometer (Hamamatsu Photonics, C11367). The X-ray-induced scintillation spectra, decay curves, and afterglow curves were measured using original setups.[47,48] The voltage and current applied to the X-ray tube for obtaining the scintillation spectra were 80 kV and 1.2 mA, respectively.

3. Results and Discussion

Figure 1 shows a photograph of the synthesized Eu-doped $CaO–Al_2O_3–B_2O_3$ glasses. Both surfaces of the glasses were polished with a polishing machine. These glasses were transparent, and the black lines behind the glasses were clearly viewed. The 10% glass was slightly pink. The weights of the glasses were 0.5026 g for the 0.1% sample, 1.1275 g for the 1% sample, 0.6271 g for the 5% sample, and 1.2607 g for the 10% sample. For the following investigations, the glasses shown in Fig. 1 were used. Figure 2 shows the XRD patterns of the synthesized Eu-doped $CaO–Al_2O_3–B_2O_3$ glasses. The halo peaks were observed at 2θ = ~30° and ~50°. No sharp peaks due to a crystal phase were observed; thus, the synthesized samples were glass, not a glass ceramic or crystal. The actual concentration is considered to be lower than the nominal concentration of Eu_2O_3 owing to the presence of a residual solution in the crucible.

Figure 3 shows the PL excitation and emission spectra of Eu-doped $CaO–Al_2O_3–B_2O_3$ glasses. Sharp emission peaks were observed at ~590, ~613, ~653, and ~702 nm under the excitation wavelength of 395 nm. Sharp excitation peaks were observed at ~365, ~380, and ~395

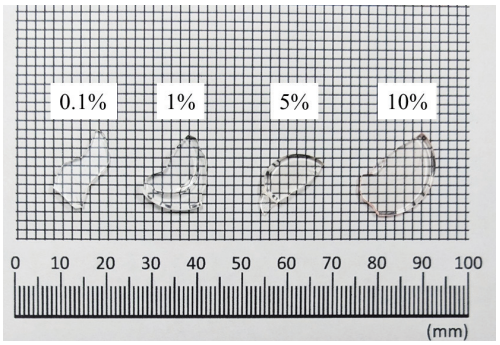

Fig. 1. (Color online) Photograph of Eu-doped $CaO–Al_2O_3–B_2O_3$ glasses.

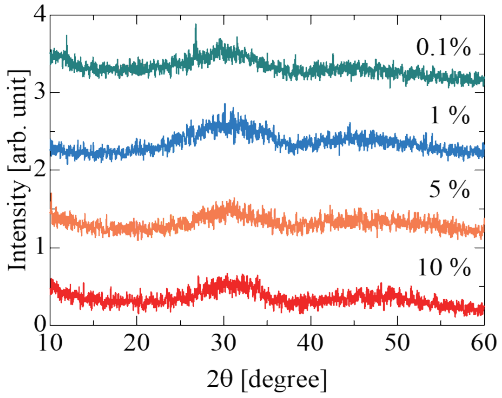

Fig. 2. (Color online) XRD patterns of Eu-doped $CaO–Al_2O_3–B_2O_3$ glasses.

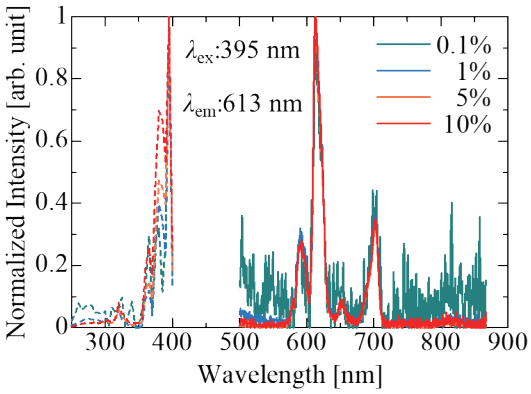

Fig. 3. PL excitation and emission spectra of Eu-doped $CaO–Al_2O_3–B_2O_3$ glasses.

nm while measuring luminescence at ~613 nm. In addition, a broad excitation band at ~280 nm was observed, the origin of which was attributed to the charge transfer of Eu^{3+}.[49] The PL QYs of Eu-doped $CaO–Al_2O_3–B_2O_3$ glasses are listed in Table 1. The PL QY increased with the Eu concentration. The PL QY of the 10% sample reached 96%. To investigate the origin of the luminescence, the PL decay curves of the Eu-doped $CaO–Al_2O_3–B_2O_3$ glasses were recorded and are shown in Fig. 4. The excitation and monitoring wavelengths were ~340 and 600 nm, respectively. The optimal excitation wavelength was 395 nm, as shown in Fig. 3, while there are sharp excitation peaks at ~340 nm. Thus, we chose ~340 nm as the excitation wavelength of PL decay. The observed PL decay curves were fitted with one exponential function. The obtained decay constants (τ_P) are listed in Table 1. The τ_P of Eu-doped $CaO–Al_2O_3–B_2O_3$ glasses in PL was ~1.8 ms, and this value was typically observed in Eu-doped materials with the 4f–4f transitions of Eu^{3+}.[50,51] Thus, the luminescence at ~600 nm was attributed to the 4f–4f transitions of Eu^{3+}.

Figure 5 shows the X-ray-induced scintillation spectra of Eu-doped $CaO–Al_2O_3–B_2O_3$ glasses. The intensity was normalized by the maximum intensity at ~613 nm. The sharp emission peaks were observed at ~600 nm, the same as in the PL spectra. In contrast, the broad emission band was observed from 300 to 500 nm in only the 0.1% sample. In a previous study, the undoped CaF_2-$Al_2O_3–B_2O_3$ glass showed a similar broad luminescence in the same wavelength region, and the origin of the luminescence was attributed to host emission.[52] The host emission was observed in only the X-ray-induced scintillation spectra, but not the PL spectra. The X-ray-induced scintillation spectra were measured by X-ray irradiation, and the X-ray energy was found to be higher than the UV energy. Usually, the energy level of the host emission center is high, and the UV energy (>250 nm) cannot reach the energy level of the host emission center. In contrast, generated carriers irradiated by X-rays can reach the energy level of the host emission center. Therefore, the broad luminescence band was observed in X-ray-induced scintillation spectra. Figure 6 shows the X-ray-induced scintillation spectra of Eu-doped $CaO–Al_2O_3–B_2O_3$ glasses. The emission intensity was corrected by the weights of the samples. The emission intensity of the 0.1% sample was low, and the 5% sample showed the highest peak intensity at ~600 nm among the synthesized samples. As the concentration of Eu increased, the peak intensity tended to increase.

Table 1
PL QY, PL decay constants, and X-ray-induced scintillation decay constants.

Sample	QY (%)	τ_P (PL) (ms)	τ_S (scintillation) (ms)
0.1%	13.5	1.8	1.1
1%	64.4	1.9	1.3
5%	78.9	1.9	1.2
10%	96.0	1.8	1.3

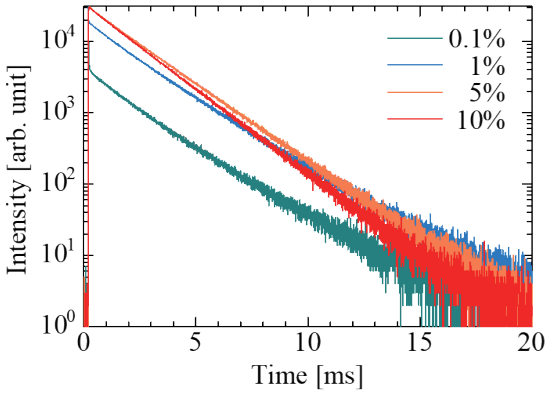

Fig. 4. PL decay curves of Eu-doped $CaO–Al_2O_3–B_2O_3$ glasses monitored at 600 nm under ~340 nm excitation.

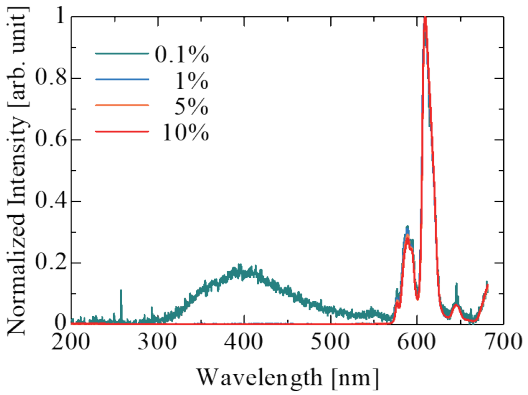

Fig. 5. X-ray-induced scintillation spectra of Eu-doped $CaO–Al_2O_3–B_2O_3$ glasses with intensity normalized by peak intensity.

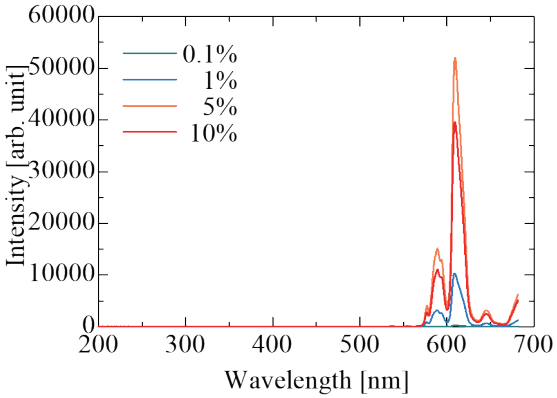

Fig. 6. X-ray-induced scintillation spectra of Eu-doped $CaO–Al_2O_3–B_2O_3$ glasses with intensity corrected by weights of samples.

Figure 7 shows the X-ray-induced scintillation decay curves of Eu-doped $CaO–Al_2O_3–B_2O_3$ glasses as well as an instrumental response function (IRF). The measured decay curves were fitted with a sum of two exponential functions. Table 1 lists the obtained scintillation decay constants. The primary decay component was removed from Table 1 because the component was due to the IRF, and the secondary decay component (τ_S) was ~1.2 ms. The value of τ_S was similar to that of the 4f–4f transition of Eu^{3+} in scintillation.[53] Judging from the spectral shape shown in Fig. 5 and the value of τ_S, the origin of the luminescence was attributed to the 4f–4f transition of Eu^{3+}. Figure 8 shows the PL QY and the X-ray-induced scintillation intensity. The value of the X-ray-induced scintillation intensity was represented by the peak intensity at ~610 nm. The PL

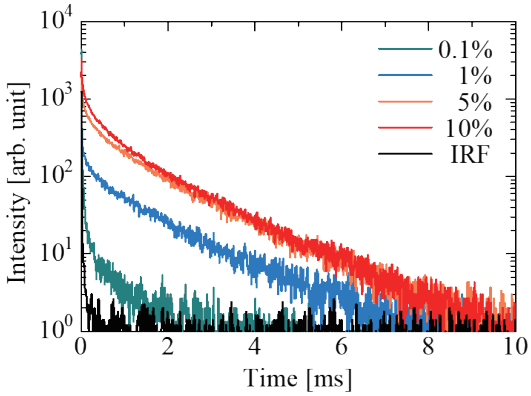

Fig. 7. X-ray-induced scintillation decay curves of Eu-doped $CaO–Al_2O_3–B_2O_3$ glasses.

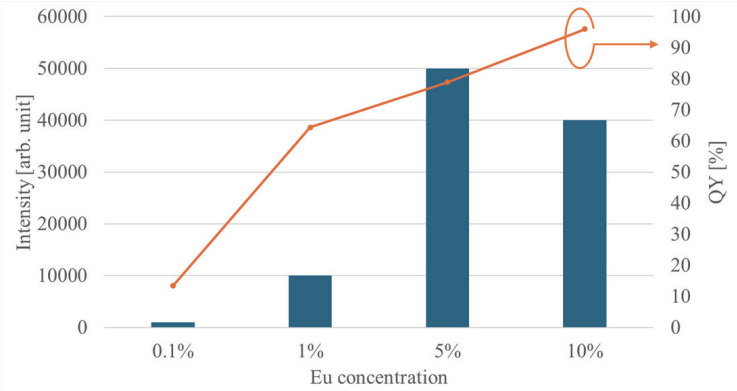

Fig. 8. X-ray-induced scintillation intensity and PL QY of Eu-doped $CaO–Al_2O_3–B_2O_3$ glasses.

QY tended to increase with the Eu concentration. The X-ray-induced scintillation intensity also showed a similar tendency, but the maximum peak intensity was observed in the 5% sample, although the maximum PL QY was obtained in the 10% sample. The X-ray-induced scintillation is emitted through the emission center, and the emission intensity depends on the PL QY. In addition, the scintillation intensity depends on not only the PL QY but also the efficiency of carrier transfer. In Robbin's model, the scintillation light yield depends on the bandgap, PL QY, and the efficiency of carrier transfer from the host to the emission center.(54) The bandgap energy was almost the same in all the samples, and the PL QY of the 5% sample was lower than that of the 10% sample. Thus, the efficiency of carrier transfer of the 5% sample was higher than that of the 10% sample. A direct observation of the efficiency of carrier transfer was difficult, but the efficiency of carrier transfer could be estimated by measuring the thermally stimulated luminescence and afterglow curve. We will measure these properties to confirm the implications of the efficiency of carrier transfer in the future.

4. Conclusions

Eu-doped $CaO–Al_2O_3–B_2O_3$ glasses were successfully synthesized by the melt-quenching method, and their luminescence properties under UV and X-ray irradiations were investigated.

Both the PL and X-ray-induced scintillation spectra showed sharp emission peaks in the red color region owing to the 4f–4f transition of Eu^{3+}. The PL and X-ray-induced scintillation decay curves supported the fact that the luminescence origin of Eu-doped $CaO–Al_2O_3–B_2O_3$ glasses was the 4f–4f transition of Eu^{3+}. The PL QY reached 96% in the 10% Eu-doped sample. The X-ray-induced scintillation intensity tended to increase with the Eu concentration.

Acknowledgments

This work was supported by the Takeuchi Ikuei Shogakukai Foundation, Cooperative Research Project of the Research Center for Biomedical Engineering, and Nuclear Regulation Human Resource Development Program/Student Research Projects.

References

1 W. Rossner and B. C. Grabmaier: J. Lumin. **48**–**49** (1991) 29. https://doi.org/10.1016/0022-2313(91)90072-4
2 C. W. E van Eijk: Phys. Med. Biol. **47** (2002) R85. https://doi.org/10.1088/0031-9155/47/8/201
3 G. Harding: Radiat. Phys. Chem. **71** (2004) 869. https://doi.org/10.1016/j.radphyschem.2004.04.111
4 K. Saito, I. Tanihata, M. Fujiwara, T. Saito, S. Shimoura, T. Otsuka, Y. Onda, M. Hoshi, Y. Ikeuchi, F. Takahashi, N. Kinouchi, J. Saegusa, A. Seki, H. Takemiya, and T. Shibata: J. Environ. Radioact. **139** (2015) 308. https://doi.org/10.1016/j.jenvrad.2014.02.014
5 T. Yanagida, Y. Fujimoto, S. Kurosawa, K. Kamada, H. Takahashi, Y. Fukazawa, M. Nikl, and V. Chani: Jpn. J. Appl. Phys. **52** (2013) 076401. https://doi.org/10.7567/JJAP.52.076401
6 T. Yanagida, T. Kato, D. Nakauchi, and N. Kawaguchi: Jpn. J. Appl. Phys. **62** (2023) 010508. https://doi.org/10.35848/1347-4065/ac9026.
7 M. J. Weber and R. R. Monchamp: J. Appl. Phys. **44** (1973) 5495. https://doi.org/10.1063/1.1662183
8 C. L. Melcher and J. S. Schweitzer: IEEE Trans. Nucl. Sci. **39** (1992) 502. https://doi.org/10.1109/23.159655
9 K. Yamabayashi, K. Okazaki, D. Nakauchi, T. Kato, N. Kawaguchi, and T. Yanagida: Sens. Mater. **36** (2024) 523. https://doi.org/10.18494/SAM4760
10 K. Miyazaki, D. Nakauchi, T. Kato, N. Kawaguchi, and T. Yanagida: Sens. Mater. **36** (2024) 515. https://doi.org/10.18494/SAM4756
11 H. Kimura, H. Fukushima, K. Watanabe, T. Fujiwara, H. Kato, M. Tanaka, T. Kato, D. Nakauchi, N. Kawaguchi, and T. Yanagida: Sens. Mater. **36** (2024) 507. https://doi.org/10.18494/SAM4767
12 R. Tsubouchi, H. Fukushima, T. Kato, D. Nakauchi, S. Saijo, T. Matsuura, N. Kawaguchi, T. Yoneda, and T. Yanagida: Sens. Mater. **36** (2024) 481. https://doi.org/10.18494/SAM4763
13 Y. Endo, K. Ichiba, D. Nakauchi, T. Kato, N. Kawaguchi, and T. Yanagida: Sens. Mater. **36** (2024) 473. https://doi.org/10.18494/SAM4758
14 T. Kunikata, P. Kantuptim, D. Shiratori, T. Kato, D. Nakauchi, N. Kawaguchi, and T. Yanagida: Sens. Mater. **36** (2024) 457. https://doi.org/10.18494/SAM4754
15 K. Ichiba, T. Kato, D. Nakauchi, N. Kawaguchi, and T. Yanagida: Sens. Mater. **36** (2024)451. https://doi.org/10.18494/SAM4752
16 H. Ezawa, Y. Takebuchi, K. Okazaki, T. Kato, D. Nakauchi, N. Kawaguchi, and T. Yanagida: Sens. Mater. **36** (2024) 465. https://doi.org/10.18494/SAM4757
17 H. Fukushima, D. Nakauchi, T. Kato, N. Kawaguchi, and T. Yanagida: Sens. Mater. **36** (2024) 489. https://doi.org/10.18494/SAM4762
18 H. Fukushima, D. Nakauchi, T. Kato, N. Kawaguchi, and T. Yanagida: Sens. Mater. **35** (2023) 429. https://doi.org/10.18494/SAM4139
19 D. Shiratori, H. Fukushima, D. Nakauchi, T. Kato, N. Kawaguchi, and T. Yanagida: Sens. Mater. **35** (2023) 439. https://doi.org/10.18494/SAM4140
20 P. Kantuptim, T. Kato, D. Nakauchi, N. Kawaguchi, K. Watanabe, and T. Yanagida: Sens. Mater. **35** (2023)451. https://doi.org/10.18494/SAM4141
21 K. Okazaki, D. Nakauchi, H. Fukushima, T. Kato, N. Kawaguchi, and T. Yanagida: Sens. Mater. **35** (2023) 459. https://doi.org/10.18494/SAM4144
22 S. Otake, H. Sakaguchi, Y. Yoshikawa, T. Kato, D. Nakauchi, N. Kawaguchi, and T. Yanagida: Sens. Mater. **36** (2024) 539. https://doi.org/10.18494/SAM4759

23 T. Kato, D. Nakauchi, N. Kawaguchi, and T. Yanagida: Sens. Mater. **36** (2024) 531. https://doi.org/10.18494/SAM4749
24 D. Shiratori, H. Kimura, Y. Fukuchi, and T. Yanagida: Sens. Mater. **36** (2024) 547. https://doi.org/10.18494/SAM4764
25 T. Kato, H. Kimura, K. Okazaki, D. Nakauchi, N. Kawaguchi, and T. Yanagida: Sens. Mater. **35** (2023) 483. https://doi.org/10.18494/SAM4137
26 D. Nakauchi, F. Nakamura, T. Kato, N. Kawaguchi, and T. Yanagida: Sens. Mater. **35** (2023) 467. https://doi.org/10.18494/SAM4138
27 T. Kunikata, T. Kato, D. Shiratori, P. Kantuptim, D. Nakauchi, N. Kawaguchi, and T. Yanagida: Sens. Mater. **35** (2023) 491. https://doi.org/10.18494/SAM4145
28 A. Nishikawa, D. Shiratori, T. Kato, D. Nakauchi, N. Kawaguchi, and T. Yanagida: Sens. Mater. **36** (2024) 597. https://doi.org/10.18494/SAM4755
29 K. Okazaki, D. Nakauchi, A. Nishikawa, T. Kato, N. Kawaguchi, and T. Yanagida: Sens. Mater. **36** (2024) 587. https://doi.org/10.18494/SAM4753
30 Y. Takebuchi, A. Masuno, D. Shiratori, K. Ichiba, A. Nishikawa, T. Kato, D. Nakauchi, N. Kawaguchi, and T. Yanagida: Sens. Mater. **36** (2024) 579. https://doi.org/10.18494/SAM4751
31 D. Nakauchi, H. Kimura, D. Shiratori, T. Kato, N. Kawaguchi, and T. Yanagida: Sens. Mater. **36** (2024) 573. https://doi.org/10.18494/SAM4750
32 N. Kawaguchi, K. Watanabe, D. Shiratori, T. Kato, D. Nakauchi, and T. Yanagida: Sens. Mater. **35** (2023) 499. https://doi.org/10.18494/SAM4136
33 Y. Takebuchi, D. Shiratori, T. Kato, D. Nakauchi, N. Kawaguchi, and T. Yanagida: Sens. Mater. **35** (2023) 507. https://doi.org/10.18494/SAM4142
34 H. Kimura, T. Fujiwara, M. Tanaka, T. Kato, D. Nakauchi, N. Kawaguchi, and T. Yanagida: Sens. Mater. **35** (2023) 513. https://doi.org/10.18494/SAM4146
35 C. W. E. van Eijk: Nucl. Instrum. Methods Phys. Res., Sect. A **460** (2001) 1. https://doi.org/10.1016/S0168-9002(00)01088-3
36 H. Masai and T. Yanagida: Jpn. J. Appl. Phys. **62** (2023) 010606. https://doi.org/10.35848/1347-4065/ac91b8
37 Y. Nakabayashi, Y. Fujimoto, M. Koshimizu, H. Kawamoto, and K. Asai: J. Lumin. **266** (2024) 120283. https://doi.org/10.1016/j.jlumin.2023.120283
38 Y. Nakabayashi, Y. Fujimoto, M. Koshimizu, H. Kawamoto, and K. Asai: J. Mater. Sci.: Mater. Electron. **35** (2024) 575. https://doi.org/10.1007/s10854-024-12307-y
39 Y. Nakabayashi, Y. Fujimoto, M. Koshimizu, and K. Asai: Opt. Mater. **142** (2023) 114136. https://doi.org/10.1016/j.optmat.2023.114136
40 K. Shinozaki, Y. Kitagawa, G. Okada, D. Nakauchi, N. Kawaguchi, and T. Yanagida: J. Lumin. **276** (2024) 120859. https://doi.org/10.1016/j.jlumin.2024.120859
41 Y. Fujimoto, T. Yanagida, Y. Futami, and H. Masai: Jpn. J. Appl. Phys. **53** (2014) 05FK05. https://doi.org/10.7567/JJAP.53.05FK05
42 I. Kawamura, H. Kawamoto, Y. Fujimoto, M. Koshimizu, G. Okada, Y. Koba, R. Ogawara, T. Yanagida, and K. Asai: J. Ceram. Soc. Jpn. **127** (2019) 663. https://doi.org/10.2109/jcersj2.19071
43 I. Kawamura, H. Kawamoto, Y. Fujimoto, M. Koshimizu, G. Okada, Y. Koba, R. Ogawara, M. Suda, T. Yanagida, and K. Asai: Nucl. Instrum. Methods Phys. Res., Sect. B **468** (2020) 18. https://doi.org/10.1016/j.nimb.2020.02.015
44 D. Nakauchi, T. Kato, N. Kawaguchi, and T. Yanagida: Opt. Mater. **154** (2024) 115746. https://doi.org/10.1016/j.optmat.2024.115746
45 M. S. Alekhin, R. H. P. Awater, D. A. Biner, K. W. Krämer, J. T. M. de Haas, and P. Dorenbos: J. Lumin. **167** (2015) 347. https://doi.org/10.1016/j.jlumin.2015.07.002
46 W. Wolszczak, K. W. Krämer, and P. Dorenbos: Phys. Status Solidi RRL **13** (2019) 1900158. https://doi.org/10.1002/pssr.201900158
47 T. Yanagida, Y. Fujimoto, T. Ito, K. Uchiyama, and K. Mori: Appl. Phys. Express **7** (2014) 062401. https://doi.org/10.7567/APEX.7.062401
48 T. Yanagida, K. Kamada, Y. Fujimoto, H. Yagi, and T. Yanagitani: Opt. Mater. **35** (2013) 2480. https://doi.org/10.1016/j.optmat.2013.07.002
49 K. Biswas, A. D. Sontakke, R. Sen, and K. Annapurna: J. Fluoresc. **22** (2012) 745. https://doi.org/10.1007/s10895-011-1010-4
50 A. Nishikawa, D. Shiratori, T. Kato, D. Nakauchi, N. Kawaguchi, and T. Yanagida: Ceram. Int. **50** (2024) 3772. https://doi.org/10.1016/j.ceramint.2023.11.130

51 N. Kawano, K. Shinozaki, D. Nakauchi, H. Kimura, M. Akatsuka, and T. Yanagida: Radiat. Phys. Chem. **190** (2022) 109785. https://doi.org/10.1016/j.radphyschem.2021.109785
52 T. Kato, S. Hirano, H. Samizo, G. Okada, N. Kawaguchi, K. Shinozaki, H. Masai, and T. Yanagida: J. Non-Cryst. Solids **509** (2019) 60. https://doi.org/10.1016/j.jnoncrysol.2018.12.025
53 N. Kawano, K. Shinozaki, T. Kato, D. Onoda, Y. Takebuchi, H. Fukushima, and T. Yanagida: Ceram. Int. **48** (2022) 9353. https://doi.org/10.1016/j.ceramint.2021.12.130
54 D. J. Robbins: J. Electrochem. Soc. **127** (1980) 2694. https://doi.org/10.1149/1.2129574